Annual Report
A-4699-2

ULTRAFINE MICROSTURCTURE COMPOSITES PREPARED BY CHEMICAL VAPOR DEPOSITION

W. J. Lackey, Garth B. Freeman, John A. Hanigofsky,
John R. Thompson, and Géoving J. Gérard
Georgia Tech Research Institute

Pradeep K. Agrawal and Woo Y. Lee
School of Chemical Engineering

and

Douglas J. Twait, Thomas S. Moss III, and Andrew J. Green
School of Materials Engineering
Georgia Institute of Technology

Prepared for:
Dr. Donald E. Polk
Code 1131
Office of Naval Research
800 North Quincy Street
Arlington, VA 22217-5000

Under:
Contract Number N00014-87-K-0036

Annual Report for the period January-December 1988

Approved for Public Release: Distribution is Unlimited

GEORGIA INSTITUTE OF TECHNOLOGY
A Unit of the University System of Georgia
Atlanta, Georgia 30332

GTRI
GEORGIA TECH RESEARCH INSTITUTE

TABLE OF CONTENTS

I. SUMMARY 1

II. INTRODUCTION 2

III. EXPERIMENTAL 4

IV. RESULTS AND DISCUSSION 9
BN Deposition 9
AlN Deposition 12
BN+AlN Composites 15

V. MODELING 24
Transport Phenomena and Kinetics 24
Crystal Nucleation and Growth 33
Future Modeling 36

VI. CONCLUSIONS 38

REFERENCES 39

II. INTRODUCTION

Recently, dispersed phase ceramic composites have received much attention because of their superior mechanical properties (e.g., fracture toughness, strength, hardness, resistance to wear and erosion, etc.). The performance of dispersed phase ceramic composites is strongly related to their microstructure. In general a microstructure consisting of a matrix of small equiaxed grains containing numerous uniformly dispersed small secondary particles is preferred. However, this type of structure is often difficult to obtain with conventional processing techniques such as powder blending followed by sintering or hot pressing since grain growth leads to large matrix grains and the dispersed particles tend to be too large and they segregate. A further problem in the case of powder mixtures is that it is difficult to achieve acceptably high densities by sintering for many ceramic systems.

Chemical vapor deposition (CVD) offers an alternate avenue of preparing ceramic composites by simultaneous deposition of multiple phases (i.e., codeposition). The major advantage of preparing dispersed phase ceramic composites by CVD is that mechanical as well as chemical, electrical, optical, and thermal properties of the composites can be favorably tailored by controlling the composite composition and microstructure. The desired microstructure can be fabricated by optimization of CVD process variables such as temperature, pressure, reagent concentration and flow rate. The potential for controlling deposit composition and microstructure and therefore properties offers a promising future for preparation by CVD. Prior work in preparing dispersed phase ceramic composites by CVD has been recently reviewed by Lackey et al. [1]. Even though rapid progress has been made, the preparation of such composites has been severely limited by the fact that the governing principles of the CVD codeposition processes thermodynamics, kinetics, transport phenomena, and crystal nucleation and growth are not thoroughly understood.

Therefore, the purpose of this study was to increase the basic understanding of the codeposition of dispersed phase ceramic coatings. Specifically, codeposition of boron nitride (BN) and aluminum nitride (AlN) was explored. Soft hexagonal BN acts as a lubricating phase because of its laminar structure while AlN having a wurtzite structure (distorted hexagonal) provides the necessary hardness to the composites. The BN+AlN system offers the promise of tailoring properties such as friction coefficient, hardness, and resistance to wear and erosion for possible radome, electromagnetic window, and tribological applications.

The preparation of BN by CVD has been the subject of numerous studies [2-12]. Also, the CVD of AlN has been well documented in the literature [13-19]. Composites of BN+AlN have been prepared previously by hot pressing [20]. However, to date, the codeposition of BN and AlN has not been studied. In order to provide guidance in the selection of process conditions for the deposition experiments reported in this paper, we performed numerous thermodynamic calculations using the SOLGASMIX-PV program [21]. In summary, the calculations predict that: (1) BN+AlN can be codeposited from the BCl_3+$AlCl_3$+NH_3 reactant system and (2) the preparation of BN+AlN composites ranging from 0 to 100% BN content is possible. The results of the thermodynamic calculations are discussed in detail elsewhere [22].

The present study has been conducted in the following manner. First, BN and AlN single phase coatings were prepared by CVD as well as BN+AlN composite coatings. Second, the coatings were characterized using X-ray photoelectron spectroscopy (XPS), electron microprobe, X-ray diffraction (XRD), and scanning electron microscopy (SEM). Third, the experimental and characterization results were explained on the basis of the underlying principles of kinetics and crystal nucleation and growth theory.

III. EXPERIMENTAL

As shown in Figure 1, the overall experimental arrangement consisted of: (1) a reagent supply system including stainless steel gas lines and control-valves, a stainless steel $AlCl_3$ vaporizer, and a stainless steel injector; (2) a resistively heated vertical graphite furnace (i.e., hot wall) in a gas tight, water-cooled stainless steel shell; and (3) a scrubber plus a corrosion resistant roughing pump from Leybold, Inc. (Type D16BCS). The desired flow rates of BCl_3, NH_3, H_2, and Ar were controlled by five mass flowmeters from MKS Instruments, Inc. (Type 1259B) with an MKS power source (Type 247C). Pressure in the furnace was measured by an MKS Baratron pressure gauge (Type 122A) and was controlled by an MKS pressure controller (Type 250B). Furthermore, an optical pyrometer (Ircon Co., Modline Plus, Type R) and a W-5Re/W-0Re thermocouple (Pyromation, Inc.) were used to measure the deposition temperature (exterior surface of the graphite reaction chamber) as shown in Figure 1. The thermocouple and pyrometer were periodically calibrated with a long W-5Re/W-26Re thermocouple (Pyromation, Inc.) by placing it inside the graphite chamber along the center line of the furnace. The deposition temperature was controlled by a temperature controller from Research, Inc. (Micristar, Model 828D), which was interfaced with the pyrometer and furnace power supply.

The $AlCl_3$ vaporizer was usually heated to 145°C with heater tapes providing a vapor pressure of $AlCl_3$ of about 70 torr. Since $AlCl_3$ (Fisher Scientific, 99.784%) is hydroscopic, it was always handled in an inert environment (i.e., glove-box filled with argon). An argon stream (usually 5 to 50 cm^3/min at STP) passed through the vaporizer and carried $AlCl_3$ vapor to the injector. BCl_3 (Matheson, 99.9%), NH_3 (Matheson, 99.99%), Ar (Matheson, 99.999%), and H_2 (Matheson, 99.999%) were used.

The injector contained two co-axial gas paths so NH_3/H_2 and $AlCl_3/BCl_3$ mixtures could be separately fed into the furnace without

ULTRAFINE MICROSTRUCTURE COMPOSITES PREPARED BY CHEMICAL VAPOR DEPOSITION

I. SUMMARY

This year we succeeded in preparing dispersed phase composite coatings which consist of a BN matrix containing AlN. The coatings were prepared by chemical vapor deposition. Both phases were deposited simultaneously, i.e., via a codeposition process. Guided by computerized thermodynamic calculations, ranges for deposition temperature and reagent concentration were discovered which permit deposition of the composite. Depending on process conditions, the BN and AlN can be made either amorphous or crystalline. Conditions exist where both phases can simultaneously be crystalline. A particularly interesting microstructure consists of crystalline turbostratic hexagonal BN matrix which contains numerous small (<0.1 μm diameter) AlN whiskers. The composite material which was deposited from BCl_3, $AlCl_3$, and NH_3 at 1100°C is unusually hard. Its hardness of 12.5 GPa exceeds that of hot pressed AlN. We believe that composites spanning a wide range of AlN contents can be prepared. The BN+AlN system is of interest for radomes, windows, and tribological applications.

Our ultimate goal is to develop an analytical model which relates deposition process conditions to composite composition and microstructure and therefore properties. The model is to be based on classical thermodynamics, mass transport, kinetic, and crystal nucleation and growth theory. The model will be validated by comparison to deposition experiments for the BN+AlN dispersed phase composite system. The basis for our model has been developed as described in detail in the body of this report. We have succeeded in obtaining a semiquantitative understanding of the BN+AlN codeposition process. Composite crystallinity can be predicted from the deposition temperature and the ratio of the input reagents BCl_3 and $AlCl_3$.

Annual Report
A-4699-2

ULTRAFINE MICROSTRUCTURE COMPOSITES

PREPARED BY CHEMICAL VAPOR DEPOSITION

W. J. Lackey, Garth B. Freeman, John A. Hanigofsky,
John R. Thompson, and Géoving J. Gérard
Georgia Tech Research Institute

Pradeep K. Agrawal and Woo Y. Lee
School of Chemical Engineering

and

Douglas J. Twait, Thomas S. Moss III, and Andrew J. Green
School of Materials Engineering
Georgia Institute of Technology

Prepared for
Dr. Donald E. Polk
Code 1131
Office of Naval Research
800 North Quincy Street
Arlington, VA 22217-5000

Under Contract Number N00014-87-K-0036

Annual Report for the period January-December 1988

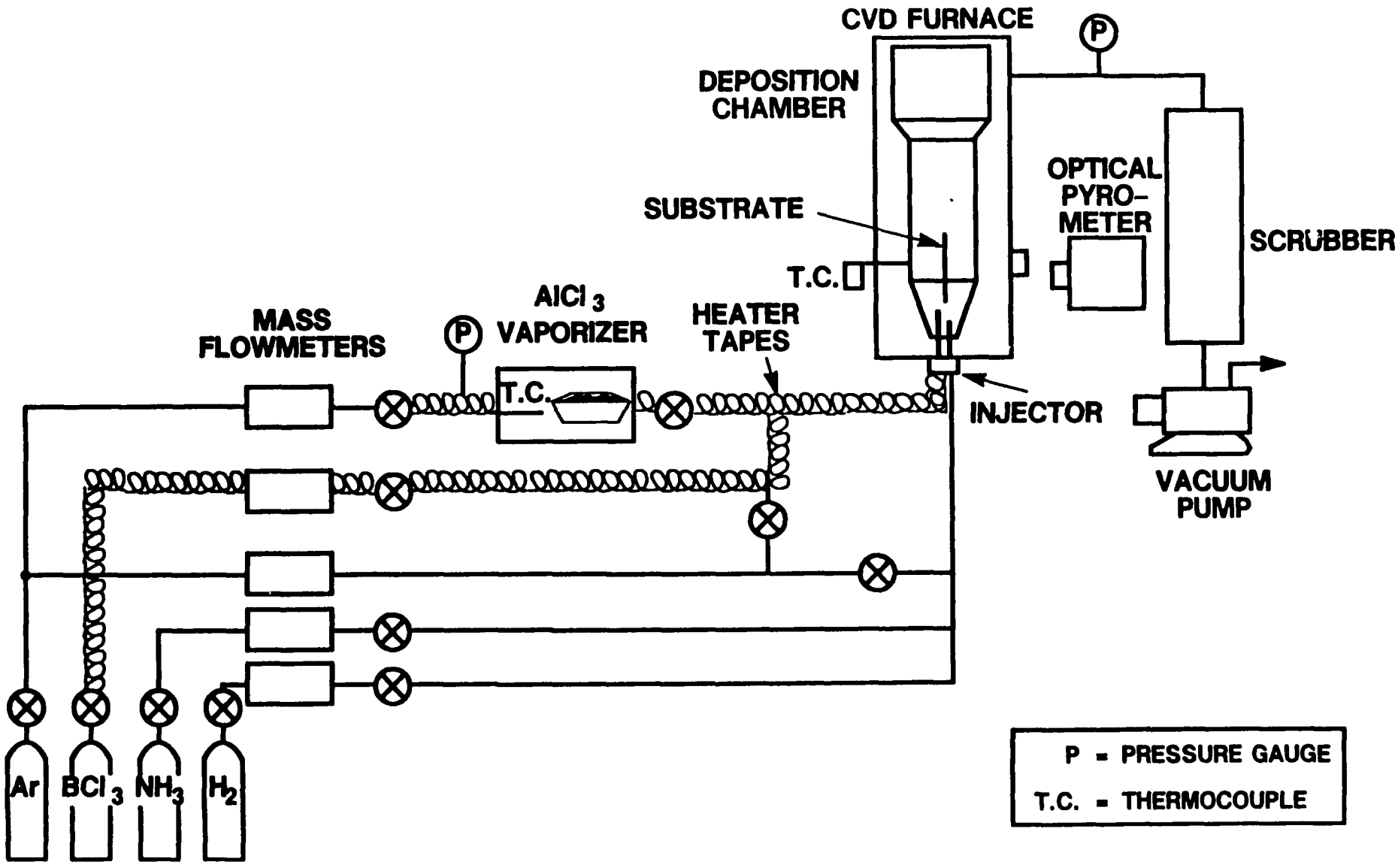

Figure 1. Schematic diagram of CVD system used to prepare BN+AlN composites.

NH_3 reacting prematurely with the metal chlorides. The two paths were usually diluted with argon. As shown in Figure 2, a graphite extension tube was used to control the mixing position of the two gas streams. The presence of a circular graphite disc with a center hole, also shown in Figure 2, forced the gas mixture to become a jet stream as the Reynolds number, Re, became larger than 140 at typical operating conditions [23]. Thus, when the substrate was placed perpendicular to the flow, a "modified impinging jet geometry" could be assumed. In most experiments, a 1.27 cm x 7.6 cm x 0.0794 cm α-Al_2O_3 strip (Coors, Type-ADS-996, 99.6 %) was either suspended vertically by molybdenum wire (Figure 3; "vertical suspension geometry") or placed horizontally on the graphite cone ("modified impinging jet geometry").

The general experimental procedure is briefly outlined as follows. The furnace was heated to the desired temperature while flowing argon at the desired pressure (usually 10.1 to 101 KPa {0.1 to 1 atm}). The deposition started when the reactants were simultaneously fed into the furnace. The deposition was terminated by stopping the reactant flows and subsequently cooling the furnace while flowing argon.

Coated substrates were X-rayed using a Philips 8000 diffractometer equipped with $Cu_{K\alpha}$ radiation operated at 40 KV. An electron microprobe analyzer (Acton MS-64 Microscope) was used to determine the elemental bulk composition (i.e., detection depth of about 1 μm). The elemental surface composition (i.e., detection depth of less than 1 nm) and the chemical bonding information were obtained using a X-ray photoelectron spectrometer from Surface Science Laboratories (Model SSX-100). Before a Cambridge 150 Steroscan scanning electron microscope was used to analyze the surface morphology, CVD coatings were coated with very thin films (e.g., less than about 20 nm) of carbon and Au/Pd to minimize the charging of highly insulating BN and AlN.

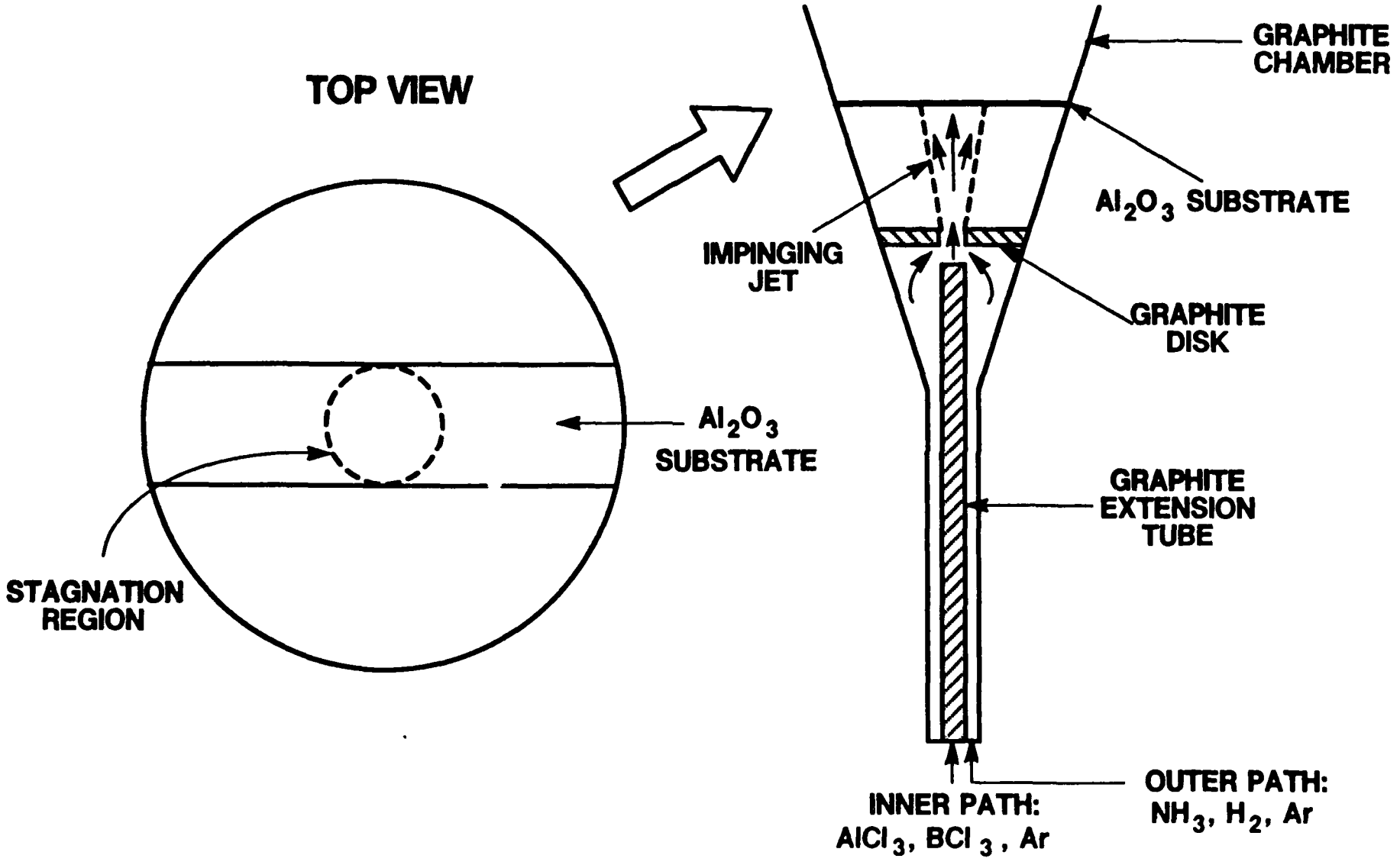

Figure 2. Modified impinging jet geometry.

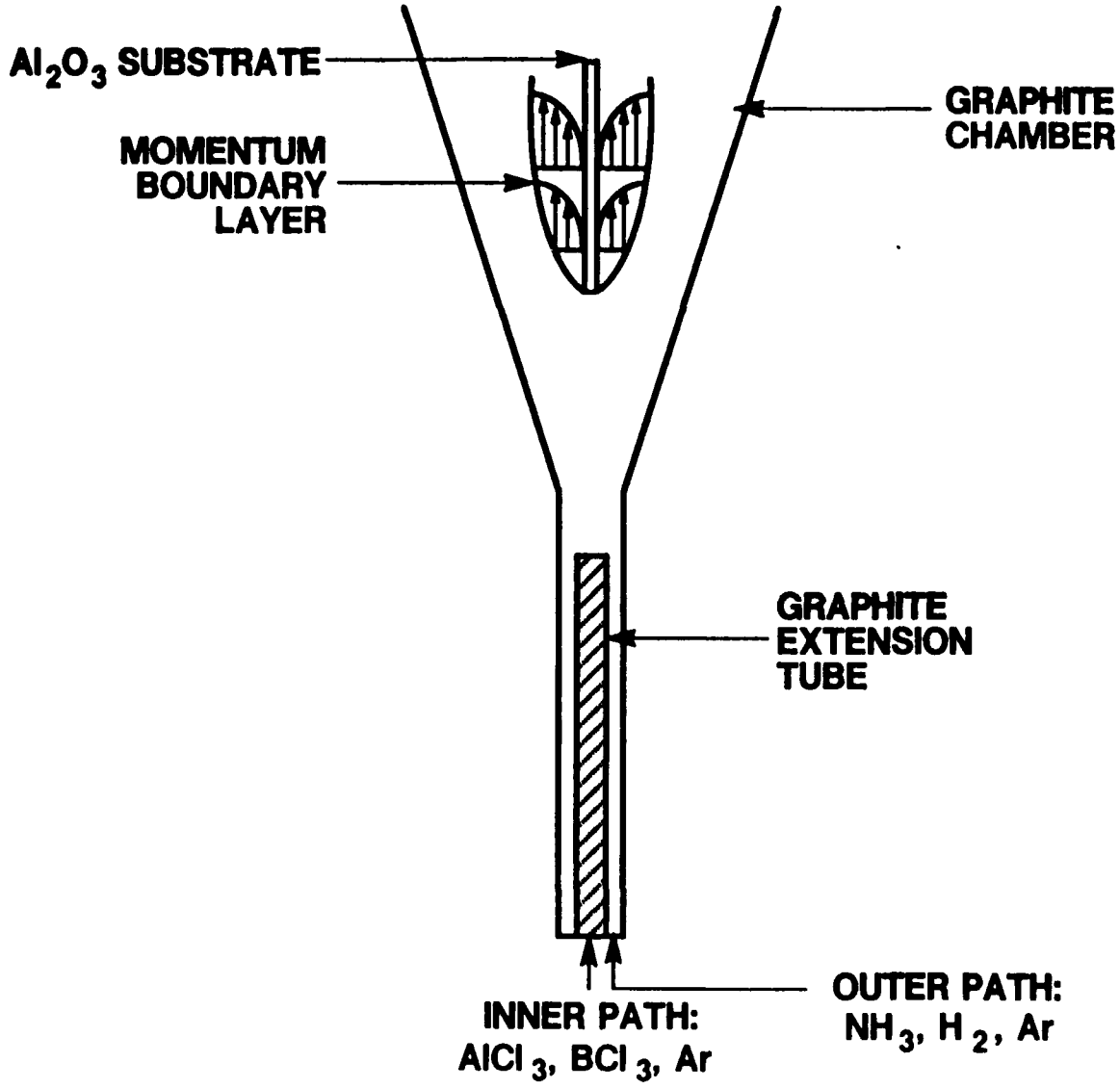

Figure 3. Vertical suspension geometry.

IV. RESULTS AND DISCUSSION

BN Deposition

Experimental conditions for nine BN experiments are shown in Table 1. All coatings obtained from these experiments contained

Table 1. Experimental conditions for BN-CVD experiments. All runs were performed for 60 minutes using the vertical suspension geometry.

Run#	T(°C)	P(atm)	Flow Rates (SCCM)				Mixing length* (cm)
			BCl_3	NH_3	H_2	Ar	
1	1200	1.0	25	100	15	500	15
2	1200	1.0	25	425	25	200	15
3	1200	0.1	25	100	25	500	15
4	700	0.2	10	50	-	400	5
5	900	0.2	10	50	-	400	5
6	1100	0.2	10	50	-	400	15
7	1100	0.2	10	50	-	400	5
8	1300	0.2	10	50	50	400	5
9	1300	0.2	10	50	50	400	5

* Distance from the mixing position of BCl_3 and NH_3 to the substrate

BN as identified by the presence of the B-N peak at 190.4 eV in the XPS spectra of these coatings. For example, Figure 4 shows an XPS spectrum of a typical BN coating and the corresponding surface and bulk elemental compositions. The presence of B_2O_3 as a minor phase on the coating surface was indicated by the appearance of the boron peak at 192.4 eV and the relatively high surface oxygen content (26.2 atomic%). However, the bulk oxygen content was much lower (2.7 atomic%) indicating that most of the B_2O_3 existed on the surface. It was suspected that most of the B_2O_3 formation was due to the surface reaction of BN upon exposure to air after the deposition process. The surface boron content was usually higher than that of nitrogen for most BN coatings. The surface boron and

	ELEMENTAL COMPOSITION (atomic%)			
	B	N	O	C
SURFACE	31.7	19.5	26.2	22.6
BULK	59.1	38.0	2.7	0.2

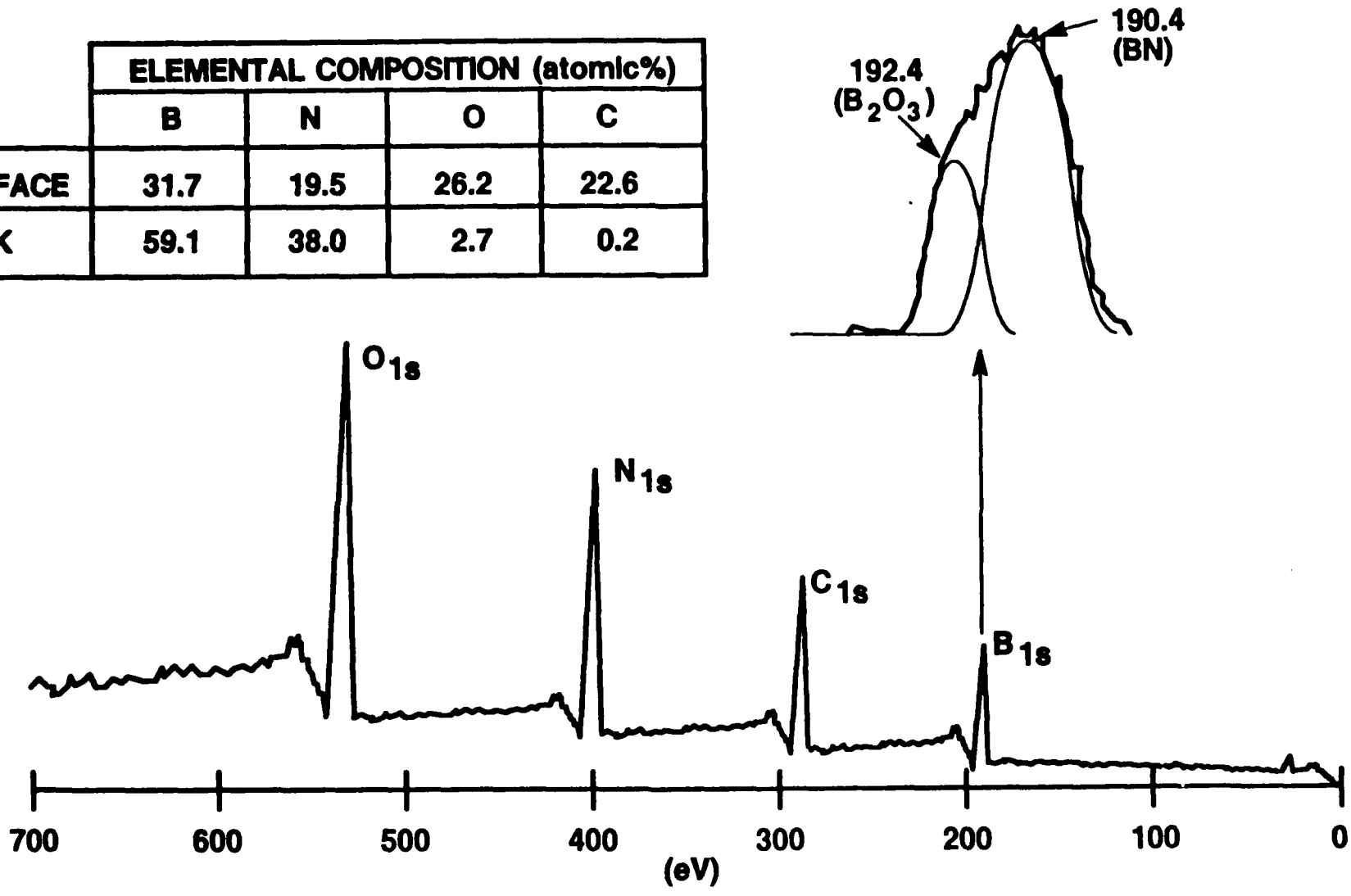

Figure 4. XPS spectrum of BN (from Run #5) and surface and bulk elemental compositions determined by XPS and electron microprobe, respectively.

nitrogen contents were not influenced in any regular fashion by the changes in operating conditions.

BN coatings which typically were powdery, soft, waxy, nonadherent white and opaque were obtained when the mixing length (i.e., distance from the mixing position of BCl_3 and NH_3 to the substrate) was 15 cm (e.g., Runs #1-4,6). The reduction of the mixing length to 5 cm produced BN coatings that were harder and more translucent and adherent. Other investigators [4,8] explained that this behavior (i.e., formation of powdery coatings) was probably due to premature reaction between BCl_3 and NH_3 to form NH_4Cl. The SEM studies showed that the hard, translucent coatings were denser than the powdery coatings.

When the mixing length was 5 cm the BN coatings became more translucent with decreasing deposition temperature; it was usually white above 1100°C, somewhat translucent at 900°C, and translucent at 700°C. The average deposition rate over the entire substrate surface ranged from 0.5 to 2.5 μm/hr. The expected Arrhenius relationship between temperature and deposition rate reported in other studies [5,7,8] was not clearly observed. The deposition rate decreased drastically along the flow direction (~100 μm/hr at the very bottom position to 0.1 μm/hr at the top); this was expected from the development of a concentration boundary layer and the depletion of the reactants.

SEM micrographs obtained from Run #5 showed that the surface morphology gradually changed along the flow direction. It changed from a fairly continuous surface containing 10 μm size nodules to a surface consisting of discrete granules of about 1 μm in size. The BN coatings having the granular morphology tended to be loose and powdery. BN coatings obtained at 101 KPa (1 atm) (Runs #1-3) generally had a very non-uniform and porous surface containing small (~0.1 μm) spherical shaped (i.e., snow-like) particles. The appearance of these particles indicated that homogeneous nucleation was probably favored at 101 KPa.

As shown in Figure 5, a very broad (002) peak (or hump) corresponding to the turbostratic BN structure [11,24] was observed at 700 and 900°C. As an approximation, an average crystallite size in the range of 1.3 to 1.8 nm was calculated based on the broadness of the (002) peaks. However, the broad (002) peak started to disappear above 1100°C and completely disappeared at 1300°C. This behavior was not in agreement with the findings of other studies in which the crystallinity of BN was found to increase with temperature [8,9]. It was proposed that at the higher temperature BCl_3 reacted with the Al_2O_3 substrate in the presence of NH_3 to form AlN as evidenced by the appearance of a small (100) AlN XRD peak (Fig. 5). Furthermore, this explanation was supported by the fact that the weight gain after the deposition was negligible.

AlN Deposition

Run conditions for AlN experiments are tabulated in Table 2. All coatings from these experiments contained AlN as determined by XPS and electron microprobe analyses. An XPS spectrum of an AlN coating is shown in Figure 6 along with the corresponding surface and bulk elemental compositions. The peak at 73.9 eV is that of AlN. The small shoulder at 72.0 eV is a charging peak. In these coatings a small amount of Al_2O_3 was occasionally detected by XPS. The bulk oxygen content determined by electron microprobe was ~6.9 atomic% con-

Table 2. Experimental conditions for AlN-CVD. All runs were performed for 60 minutes and at the mixing length (i.e., distance from the mixing position of $AlCl_3$ and NH_3 to the substrate) of 15 cm using the vertical suspension geometry.

Run#	T(°C)	P(atm)	Flow Rates (SCCM)		
			$AlCl_3$	NH_3	Ar
1	1200	1.0	3.4	100	1750
2	1200	1.0	2.9	100	1900
3	1200	1.0	5.0	100	1900
4	700	0.2	4.2	50	1500
5	900	0.2	3.8	50	1500
6	900	1.0	6.3	50	1500
7	1100	0.2	6.8	50	1500

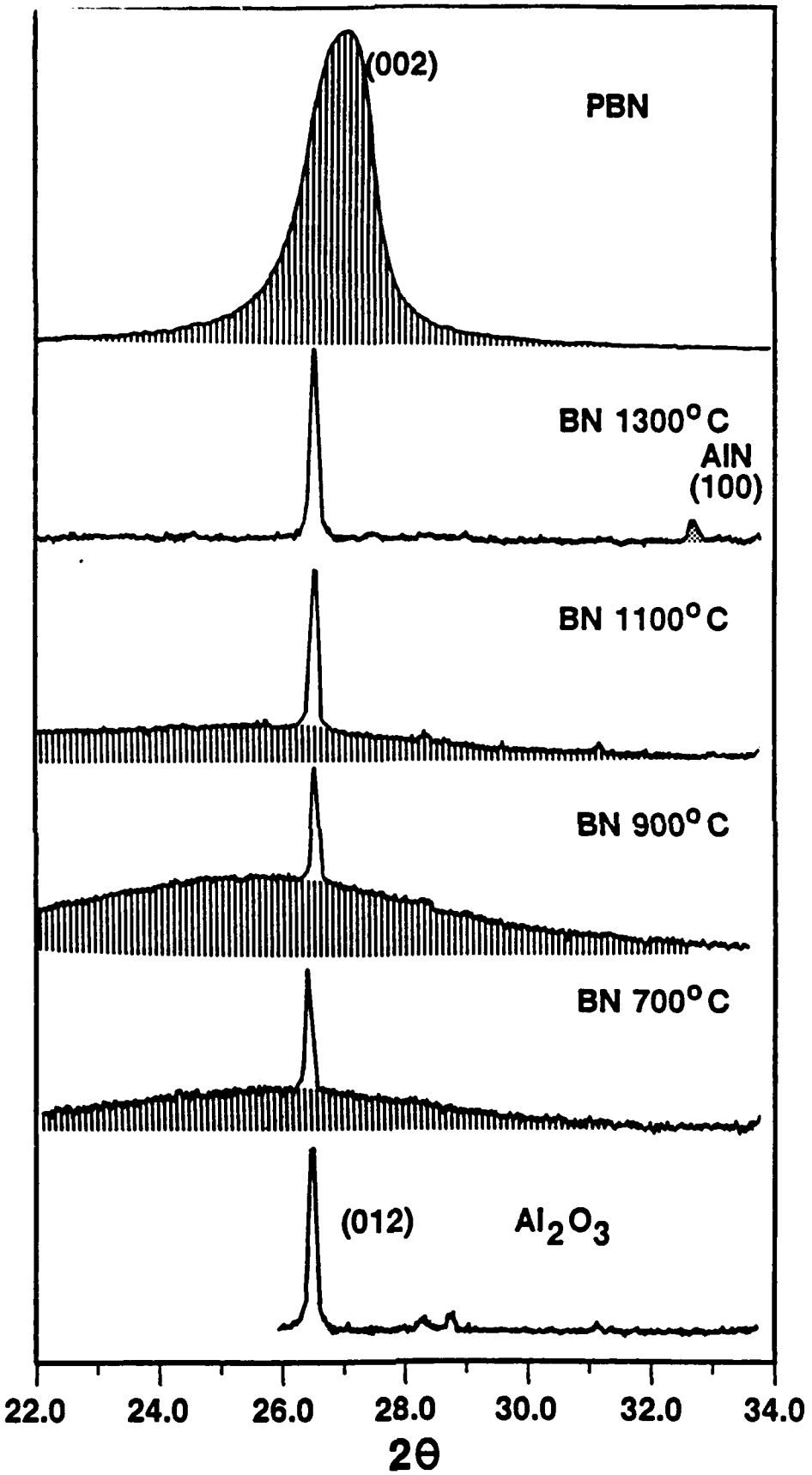

Figure 5. XRD patterns of BN deposited on Al_2O_3 at various temperatures. Top curve is for commercially prepared, highly oriented pyrolytic BN. Bottom curve is for the Al_2O_3 substrate.

	ELEMENTAL COMPOSITION (atomic%)				
	Al	N	O	C	Cl
SURFACE	29.4	15.5	21.7	32.2	1.5
BULK	31.4	60.7	6.9	0.4	0.6

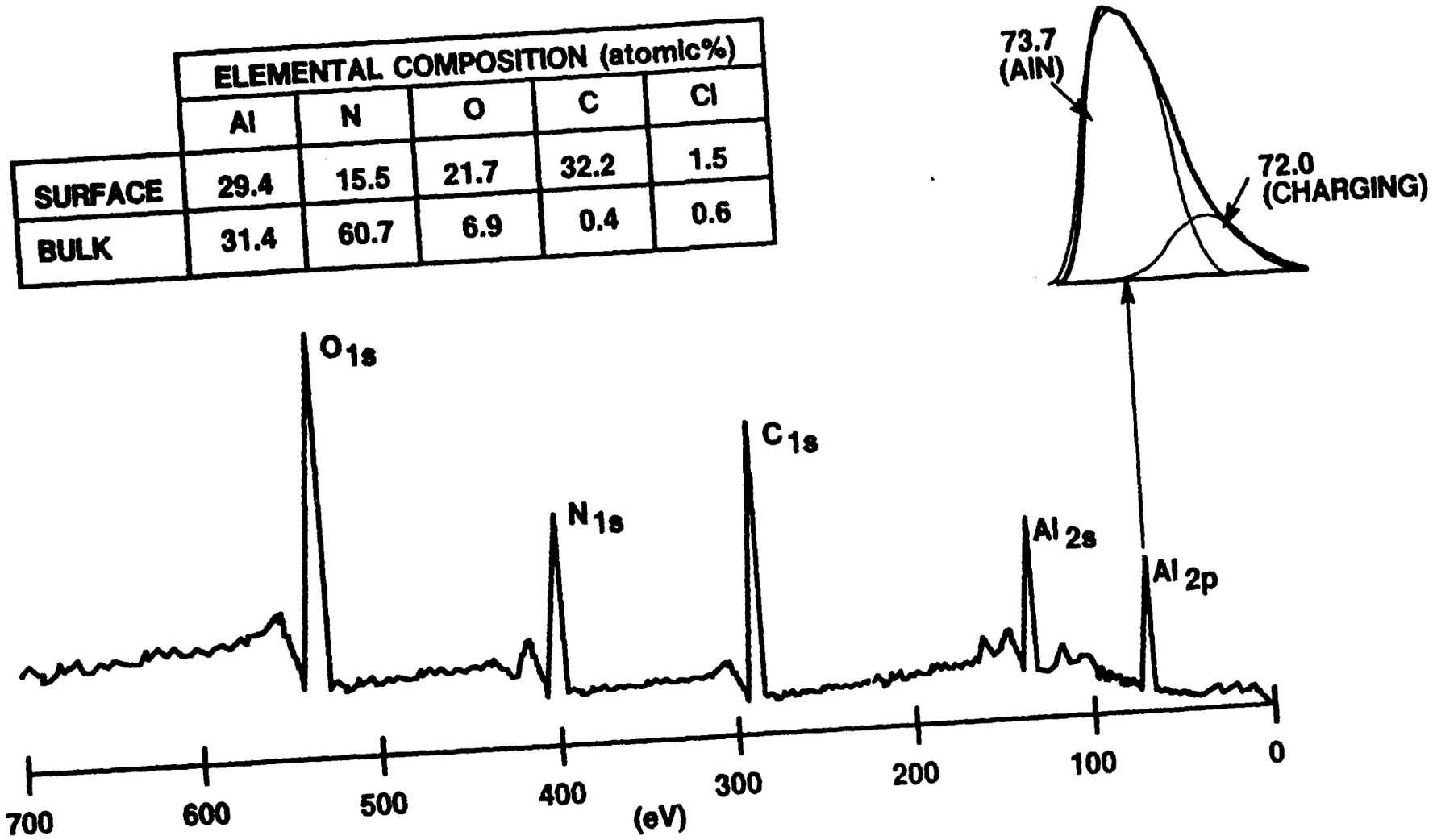

Figure 6. XPS spectrum of AlN (from Run #5) and surface and bulk elemental compositions determined by XPS and electron microprobe, respectively.

firming that AlN was actually the major phase. A higher nitrogen bulk content (~60.7 atomic%) compared to that of aluminum (~31.4 atomic%) was observed. However, the surface nitrogen content (~15.5 atomic%) was usually lower than that of aluminum (~29.4 atomic%).

The effect of the mixing length on the AlN deposition behavior was not studied. However, it is expected that the effect was minimal compared with that for BN since NH_4Cl formation from the $AlCl_3$ and NH_3 mixture is not favorable at low temperatures. The AlN coatings obtained at 1200°C and 101 KPa (Runs #1-3) were observed to be nucleated from the gas phase since non-uniformly distributed small "snow-like" particles were observed under SEM as in the case of BN deposition at 101 KPA.

As the deposition temperature was increased from 700 to 1100°C (Runs #4-7), the deposition rate decreased from 2.84 to 0.005 μm/hr. This trend was in agreement with other studies [17-19], in which it was explained that the deposition rate decreased because of the domination of homogeneous nucleation over heterogeneous nucleation above 1000°C. The coating rate was usually much higher at the bottom of the vertically suspended substrate (~100 μm/hr) than at the top (~0.1 μm/hr).

Figure 7 shows XRD spectra of AlN deposited at 700 and 900°C. No discernible AlN X-ray pattern was obtained for AlN deposited at 1100°C, as the amount of coating was insufficient. The slightly broadened AlN peaks at 700°C were assigned to randomly oriented polycrystalline AlN. The average crystallite size of about 11 nm was calculated based on the broadness of the (002) peak. At 900°C, the (002) peak predominated over the other major peaks indicating the presence of preferred orientation of the AlN grains (i.e., c-axis perpendicular to the substrate).

BN+AlN Composites

Codeposition run conditions are presented in Table 3. XPS studies indicated that all coatings obtained from the codeposition

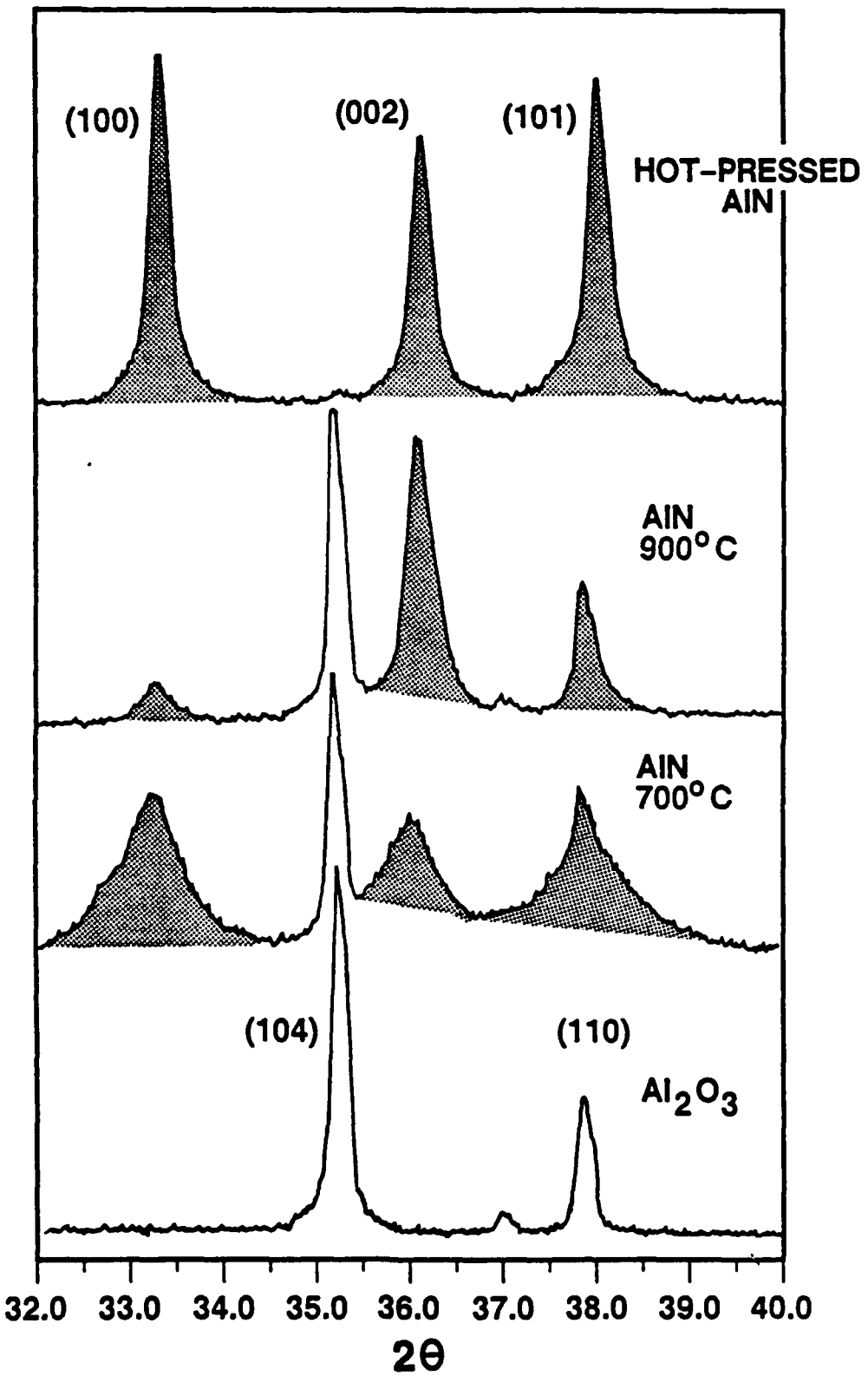

Figure 7. XRD patterns of AlN deposited on Al_2O_3 at various temperatures. Top curve is for commercially prepared AlN. Bottom curve is for the Al_2O_3 substrate.

Table 3. Experimental conditions for BN+AlN-CVD experiments.

Run#	T(°C)	P(atm)	Flow Rates (SCCM)					Run Time (min)	Mixing length* (cm)	Substrate arrangement**
			BCl_3	$AlCl_3$	NH_3	H_2	Ar			
1	1200	1.0	25	6	100	-	3200	60	15	V
2	1200	1.0	25	6	100	200	3200	60	15	V
3	1200	1.0	14	6	212	250	3200	60	15	V
4	700	1.0	10	8	50	-	1500	60	15	V
5	900	0.2	5	4	50	-	1500	120	15	V
6	900	0.2	10	1	50	-	1500	60	15	V
7	1100	0.2	10	6	50	-	1500	60	15	V
8	900	0.2	10	7	50	-	1430	90	5	V
9	900	0.2	30	6	50	100	1840	60	5	V
10	900	0.2	10	10	50	100	1940	60	5	V
11	1100	0.2	10	7	50	-	1430	60	5	V
12	1100	0.2	10	8	50	100	1330	60	5	V
13	1100	0.2	10	4	50	-	1940	60	5	V
14	727	0.2	6	21	75	100	1900	60	5	I
15	927	0.1	3	10	35	50	950	60	5	I
16	927	0.1	3	6	40	50	950	60	5	I
17	927	0.2	6	13	75	100	1900	60	5	I
18	1127	0.2	10	15	50	-	1900	60	5	I
19	1127	0.2	10	5	80	-	1900	60	5	I

* Distance from the mixing position of $BCl_3/AlCl_3$ and NH_3 to the substrate.

** V: Vertical suspension geometry
I: Modified impinging geometry

experiments contained BN and AlN as two major phases. Occasionally B_2O_3 and/or Al_2O_3 were observed on the coating surface. Figure 8 shows an XPS spectrum of a BN+AlN composite along with the corresponding surface and bulk elemental compositions. It was noted that the small peaks at 396.2 and 188.6 eV were charging peaks. The surface elemental composition of the composites determined by XPS was not affected in any regular manner by the changes in operating conditions.

As summarized in Figure 9, XRD studies showed that the crystallinity of the BN+AlN composites was strongly dependent on the deposition temperature, T, and the $P_{BCl_3}/(P_{AlCl_3} + P_{BCl_3})$ ratio, η. Even though XPS and electron microprobe studies indicated that BN and AlN were always present in these composites, the presence of both crystalline AlN and turbostratic BN was only observed when temperature was 1100°C and η was about 0.67. When η was less than about 0.6, only crystalline AlN was detected by XRD. Turbostratic BN was detected when η was higher than about 0.7 at 1100°C and 0.84 at 900°C.

A deposition mechanism which controls whether coatings are amorphous or crystalline is described in the following hypothesis. The central idea of the hypothesis is that codeposition of two chemically different phases (i.e., BN+AlN) is a competitive process in which the growth of one phase interferes with and/or limits the growth of the other. For example, it is recalled from the BN deposition studies that the average crystallite size of BN obtained at 700 to 900°C is about 1.3 to 1.8 nm. If the growth of AlN is favored over that of BN, BN grains will be "out-grown" by AlN grains and the BN grains will become even smaller in the codeposition than in the single phase deposition process. Such small BN particles are probably not large enough to be classified as turbostratic (i.e., the structure could be said to be amorphous) and thus are not detected by XRD. Physically, this corresponds to a structure where the matrix consists of numerous, very small BN particles in which are imbedded much larger AlN crystals.

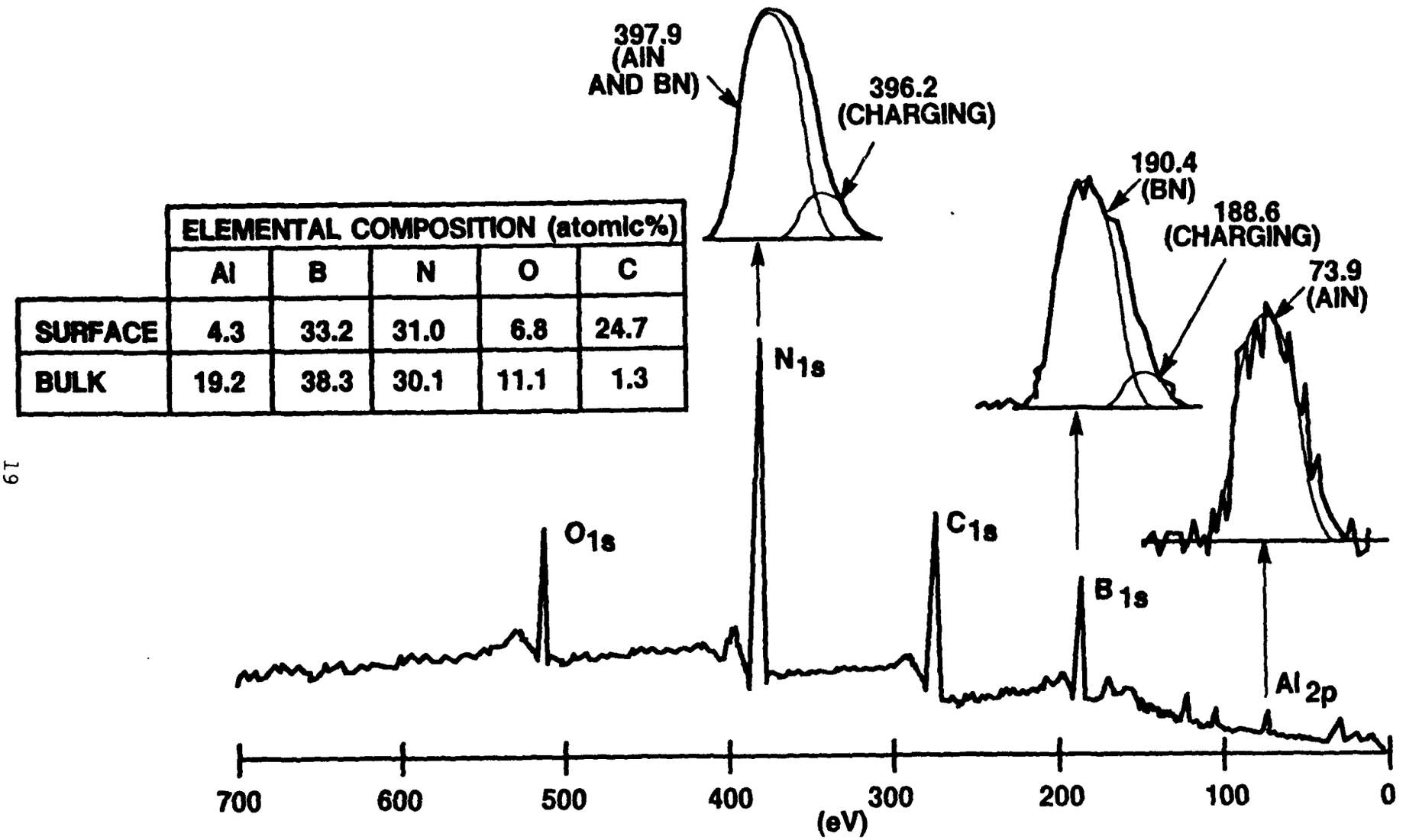

	ELEMENTAL COMPOSITION (atomic%)				
	Al	B	N	O	C
SURFACE	4.3	33.2	31.0	6.8	24.7
BULK	19.2	38.3	30.1	11.1	1.3

Figure 8. XPS spectrum of BN+AlN (from Run #7) and surface and bulk elemental compositions determined by XPS and electron microprobe, respectively.

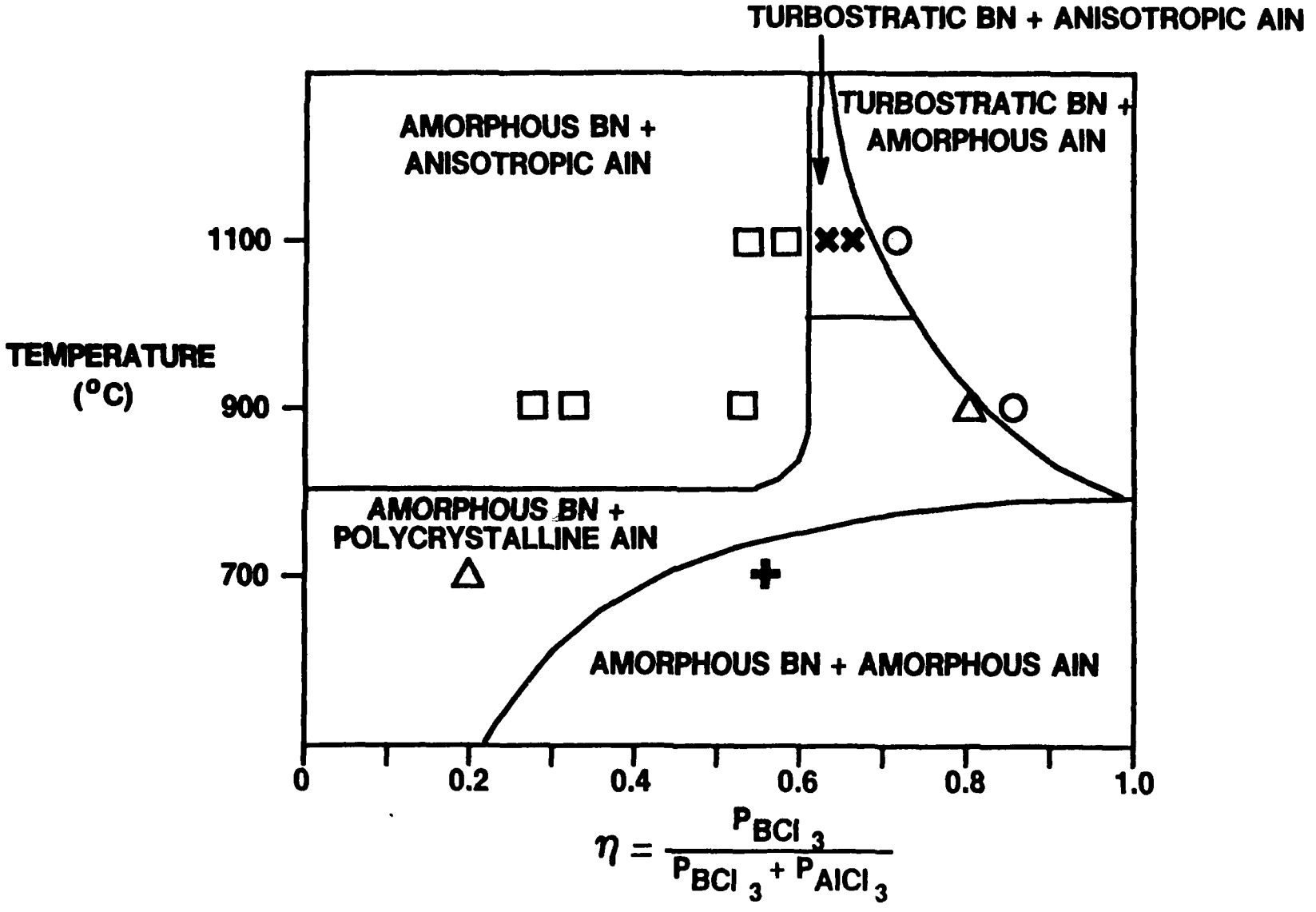

Figure 9. Microstructure of BN+AlN composites determined by XRD as a function of deposition temperatures and $AlCl_3$ and BCl_3 partial pressures.

This explanation is supported by the XRD results. The low η ratios (~0.17 to 0.50) correspond to conditions where the growth of AlN grains is favored over that of BN grains according to the statistical-mechanical nucleation and growth theory [25-28]. The theory states that the crystal growth is dependent on the surface mobility and the rate of adatom arrival onto the surface. Based on a simple kinetic approximation, it is expected that the ratio of the rate of Al adatom formation over that of B adatoms increases as η decreases. As more Al adatoms than B adatoms are arriving on the surface per given time, AlN clusters should outgrow BN clusters resulting in the larger AlN grains and limiting the further growth of the BN clusters (i.e., small BN grains) assuming the surface mobility of the Al and B adatoms are similar in magnitude. The opposite is expected to be true when η is high (~0.84). In this case, only turbostratic BN is observed. Therefore, according to the hypothesis, it is suspected that AlN grains are too small in this instance to be detected by XRD.

An optimum region of operating conditions exists for the preparation of the composites containing crystalline AlN and turbostratic BN. In this region, the growth rate of BN and AlN grains should be comparable in order to minimize the dominant growth of one phase over the other. Experimentally, this region is near 1100°C when η is about 0.67. The XRD pattern of a BN+AlN composite obtained at this region (Run #18) is shown in Figure 10.

Based on the SEM and XRD studies, it was speculated that the BN+AlN composites obtained above 900°C structurally consisted of fine AlN whiskers oriented generally perpendicular to the deposition surface. The AlN whiskers were embedded in a matrix of very small BN particles. For example, a composite containing turbostratic BN and anisotropic AlN is ideally represented in Figure 11. The composite contained: (1) AlN grains that were preferentially oriented with c-axis orientation and about 11 nm in diameter and (2) BN grains about 1.5 nm in diameter. The above BN and AlN crystallite sizes were calculated from the broadening of their (002)

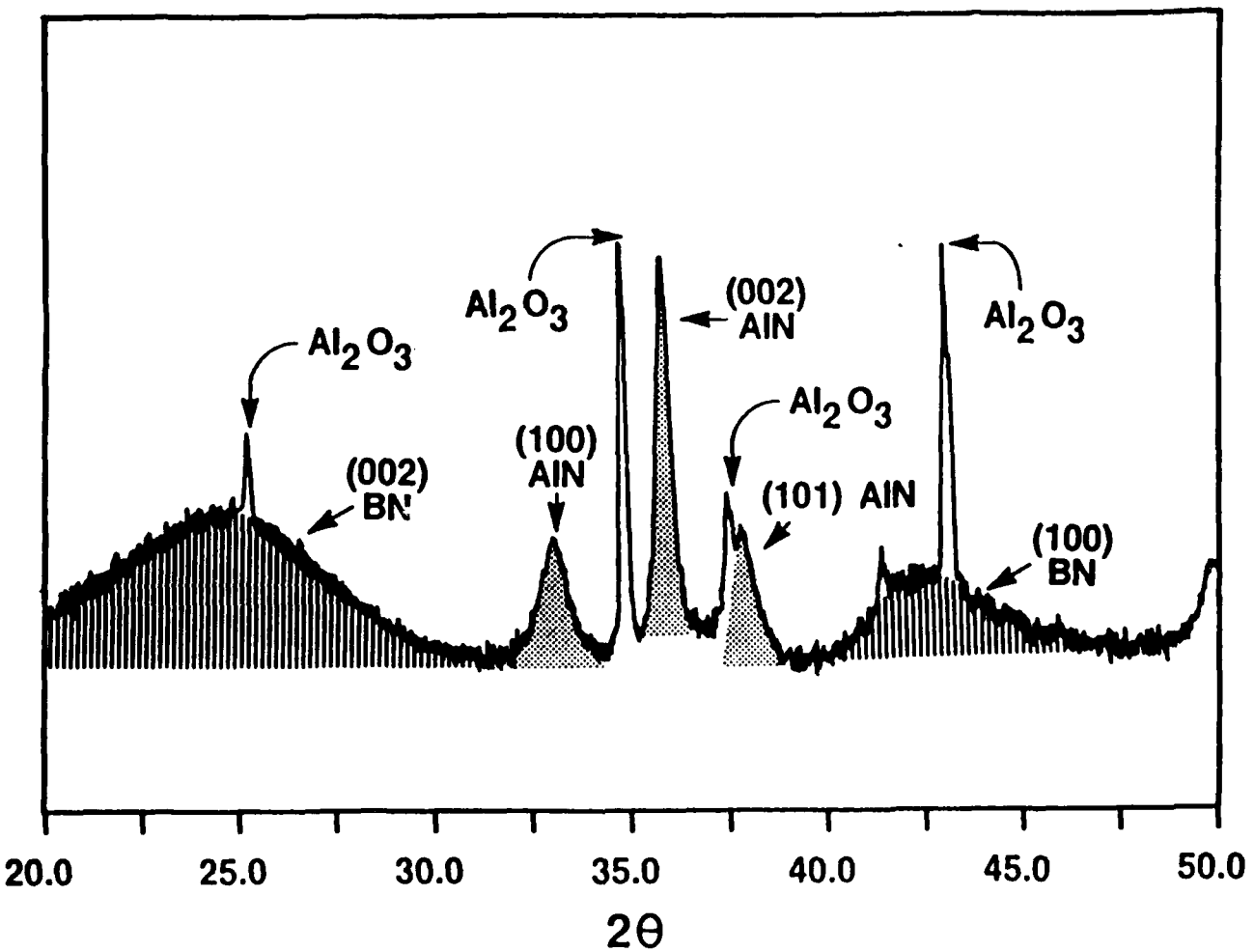

Figure 10. XRD pattern of BN+AlN composite containing turbostratic BN and anisotropic AlN (from Run #18).

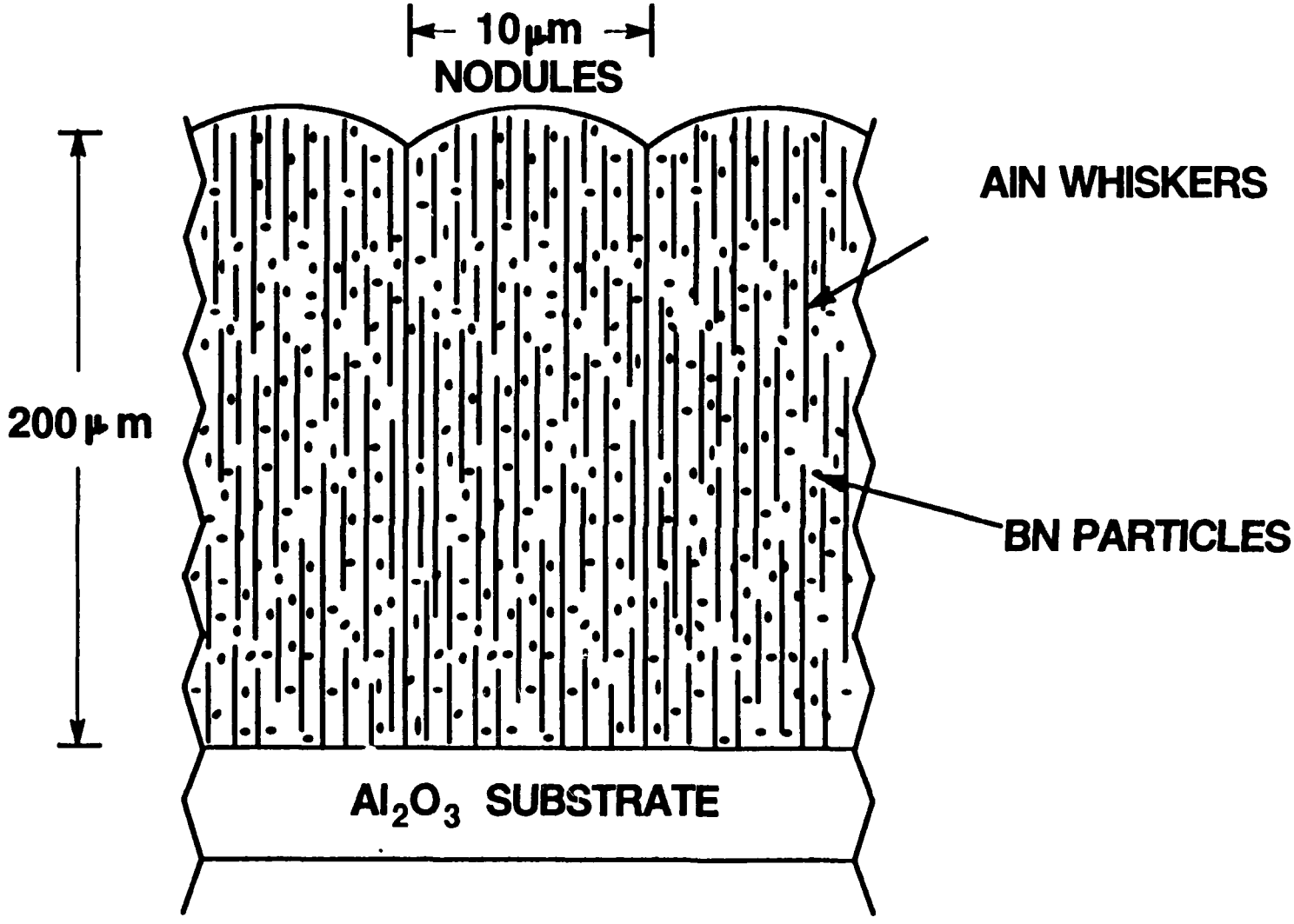

Figure 11. Ideal representation of a composite containing turbostratic BN and anisotropic AlN.

peaks. TEM micrographs corresponding to this structure are shown in Figure 12.

Apparently, the nucleation and growth behavior of BN and AlN was altered in the codeposition process (i.e., BN+AlN-CVD) in comparison to the single phase deposition processes (i.e., BN-CVD and AlN-CVD). At 700°C the composite was amorphous despite the fact that turbostratic BN from the BN-CVD and polycrystalline AlN from AlN-CVD were deposited at the same temperature. Most interestingly, AlN was deposited at 1100°C in the codeposition process whereas AlN was not deposited above 900°C in the AlN-CVD experiments.

Much thicker coatings were obtained with the impinging jet geometry (~200 μm/hr) than with the vertical suspension geometry (~20 μm/hr). The coatings obtained in the stagnation region (a region ~1 cm diameter) were uniform. These results supported the validity of the modified impinging jet arrangement.

The total weight gain decreased by a factor of two as temperature increased from 900 to 1100°C. The magnitude of the weight gain was similar to that for BN-CVD experiments. The BN+AlN composites became less translucent with increasing temperature. Coatings were transparent at 700°C, translucent at 900°C and somewhat translucent at 1100°C. In general, the coatings were harder than commercially available pyrolytic boron nitride and hot pressed aluminum nitride as shown in Figure 13.

V. MODELING

Transport Phenomena and Kinetics

A comprehensive CVD model, which predicts the deposition rate from a given set of operating conditions, involves momentum, energy, and mass (species) balances as well as kinetic rate expressions. Mathematically, this means that a set of coupled-partial (or ordinary) differential equations is required. Kinetics of the process are incorporated into the model as depletion or

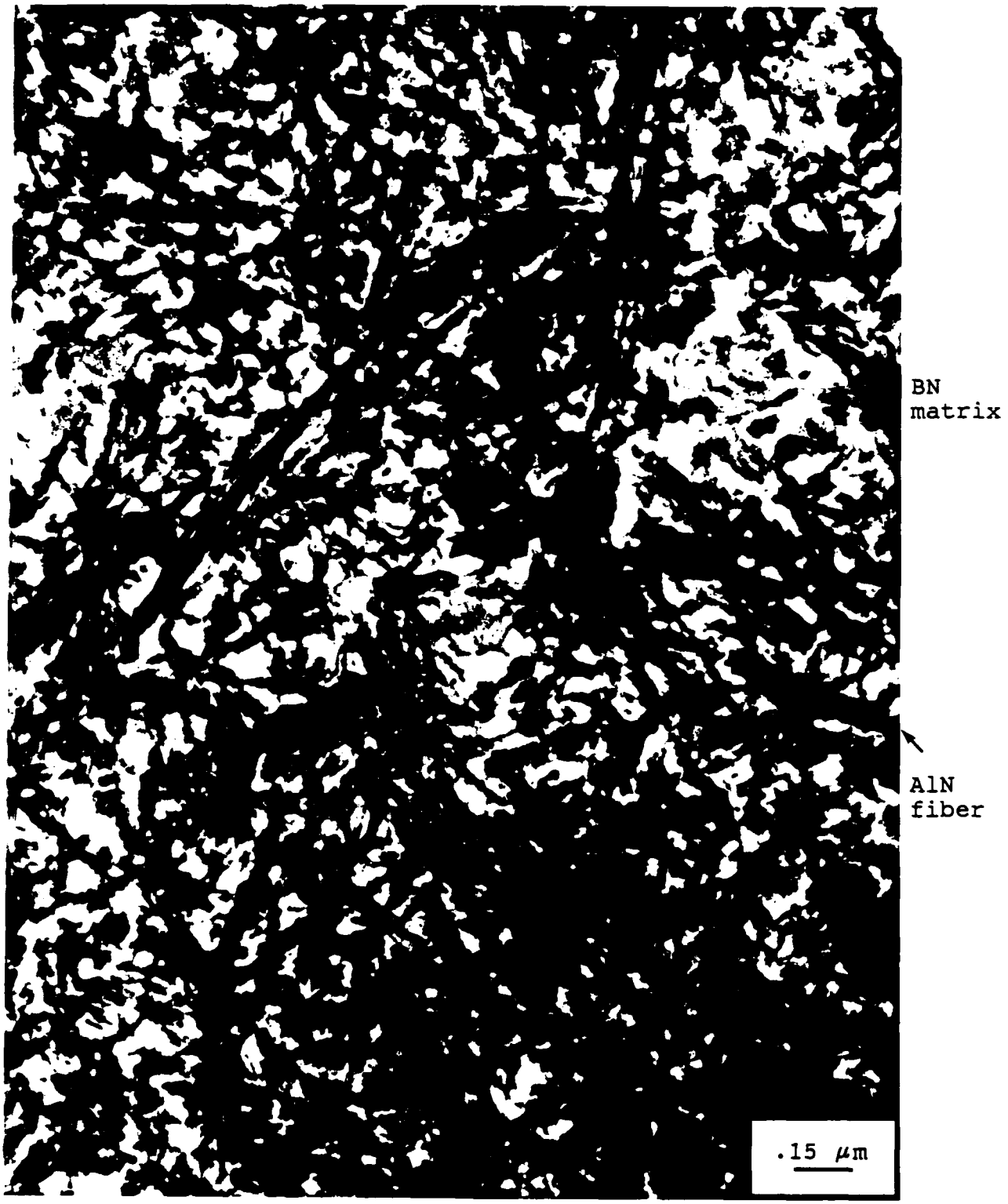

Figure 12. TEM micrograph containing anisotropic AlN fibers surrounded by a BN matrix.

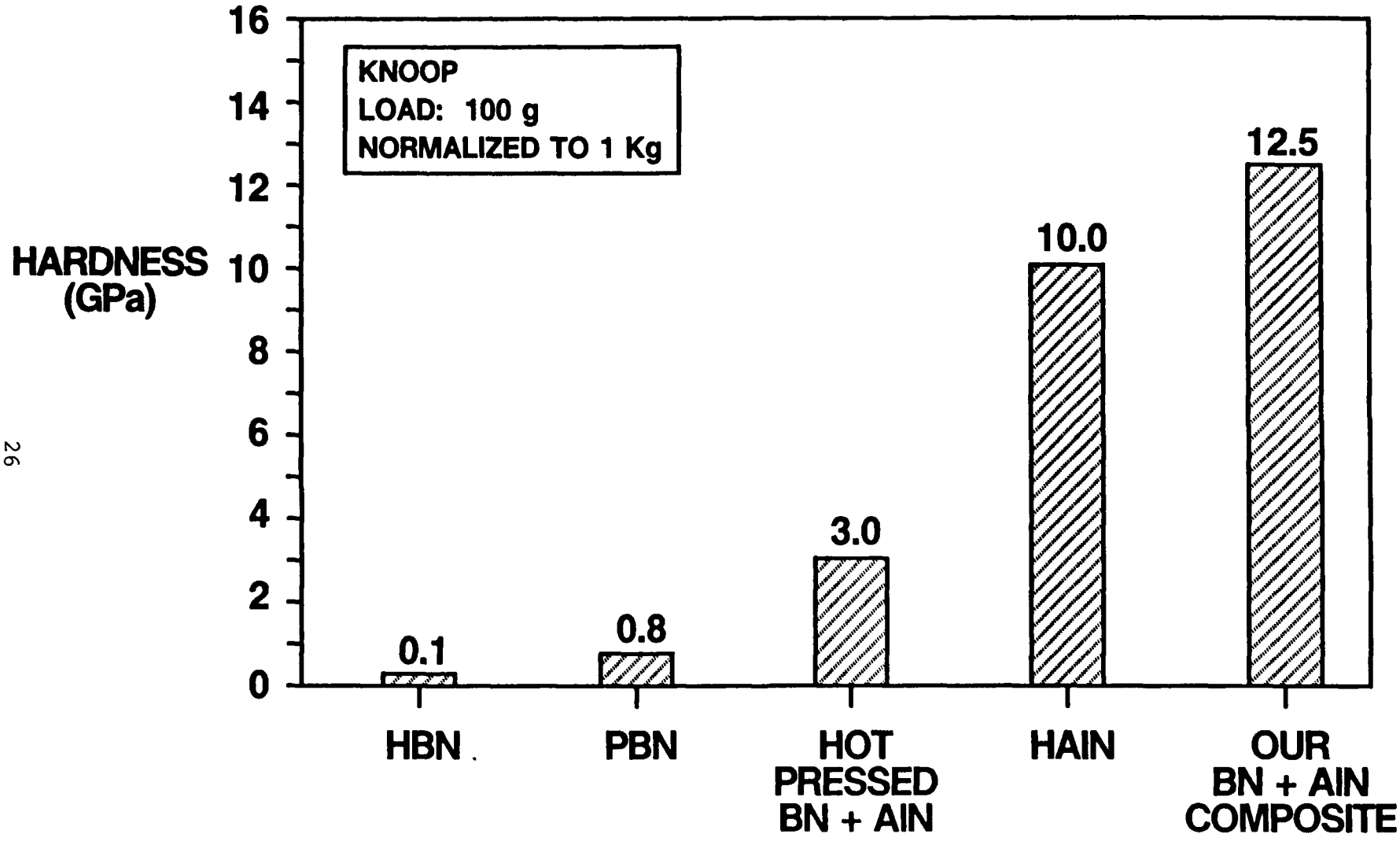

Figure 13. Hardness comparison between various AlN, BN, and AlN+BN composites.

production terms in the species balances for homogeneous reactions and as boundary conditions of the species balances for heterogeneous reactions. The general forms of these equations have been previously derived [29-32]. Therefore, the objective of this section is not to reiterate these equations, but to present possible assumptions and simplifications that are applicable to the BN+AlN system and the resulting equations.

One of the most important goals of the simplification process is to reduce the mathematical complexity to a level where the influence of operating conditions (e.g., reactant concentrations) on the deposition rate can be readily understood without having to perform a rigorous fitting of kinetic parameters. This philosophical approach can be best illustrated by considering the following example. To date two "sophisticated" mathematical CVD models have been developed. Rebenne and Pollard [32] have solved momentum, energy, and mass balances using a finite difference method to describe experimental results obtained by Vandenbulcke [33,34] on CVD of boron carbide in an impinging jet reactor. Roenigk and Jensen [35,36] have developed a two-dimensional model for low pressure chemical vapor deposition (LPCVD) of silicon and silicon nitride in a "hot-wall multiple-wafers-in-tube" reactor using an orthogonal collocation method. This model predicts the effects of operating conditions on the deposition rate at various substrate positions. However, in both studies, the predictive capability of the models over a wide range of operating conditions was questionable since Rebenne and Pollard had 24 adjustable parameters and Roenigk and Jensen used 12 adjustable parameters for the Si_3N_4-LPCVD system without having much of the necessary kinetic data. This type of investigation involving model discrimination and parameter estimation usually requires the accompaniment of extensive experimental work and statistical testing [37]. In the case of the silicon deposition, "educated guesses" in estimating kinetic parameters were possible, however, because reaction mechanisms of the Si-CVD system were relatively well-understood through numerous

experimental studies performed on this comparatively simple system. Therefore, it is concluded that this "sophisticated" mathematical approach is suitable for simple and well-understood CVD processes. However, this approach loses its merit for complex systems as the true physicochemical nature of the processes may be lost during the empirical fitting process of numerous kinetic parameters unless a significant amount of kinetic data is available.

In comparison to the above mentioned CVD systems, the BN+AlN system is much more complex because more chemical species and phases are involved. In addition, the BN+AlN CVD system has never been studied previously. Therefore, it should be the first priority to obtain intrinsic kinetic data of this system. This kinetic study should be done in a simple and well-understood reactor geometry to minimize other complications such as non-uniform flow patterns and mass transfer. Then, the kinetic data can be interpreted by a simplistic but reasonable kinetic/diffusion model (e.g., semi-quantitative to qualitative modeling).

A modified impinging jet geometry is chosen for the proposed work (see Section III for experimental details) since its hydrodynamics is well-understood [38-40]. The geometry has been recognized as an ideal reactor design for obtaining accurate kinetic data [30,41]. The reactant gas mixture (i.e., jet) flows perpendicular to the substrate and then flows away radially. The vicinity of the substrate surface where mass transfer is independent of radial position is called the stagnation region. In this region, it is determined experimentally as well as theoretically that one-dimensional analysis (i.e., function of z only) is adequate to explain deposition data [33-36,41-44]. Inside the stagnation region, a thin layer of momentum boundary with a constant thickness, δ_m, exists near the substrate surface along the radial direction.

Using this impinging geometry, an idealized situation for CVD of BN+AlN from the BCl_3+$AlCl_3$+NH_3+Ar reactant mixture is considered in order to illustrate how a simple qualitative model can provide

physical insights to the process. First, the following assumptions and/or simplifications are made:

(1) The energy balance is not considered. This is a valid assumption when a hot wall reactor is used (i.e., constant temperature profile in the vicinity of the substrate) [30]. It is calculated that heat generated at the substrate surface as BN forms (i.e., exothermic reaction) only causes a small temperature increase of about 32°C [29]. Furthermore, this temperature increase is effectively compensated by the slightly endothermic AlN reaction.

(2) Because of assumption (1), constant physical properties can be assumed.

(3) Reactants from the nozzle to near the deposition surface are transferred by convection only. This assumption is valid since the Peclet number, Pe, is about 360 to 1500 at typical operating conditions (i.e., mass transfer by convection is much larger than that by molecular diffusion). The Peclet number is defined here as

$$Pe = \frac{v\,H}{D_{im}} \qquad (1)$$

where v is the linear velocity of the jet stream, H is the distance from the nozzle to the deposition surface, and D_{im} is the diffusion coefficient of gas species i in the fluid mixture. Therefore, the concentration composition in the gas phase near the deposition surface is identical to that of the inlet condition as long as there is no homogeneous reaction, since convection is an efficient means of mass transfer.

(4) The diffusion of BCl_3 through the concentration boundary layer and the surface decomposition of BCl_3 at the deposition surface are two processes in series, which determine the overall BN deposition rate while the same assumption applies to $AlCl_3$ in the case of AlN deposition. This is equivalent to saying that either: (1) there are no homogeneous reactions

or (2) homogeneous reactions are fast compared to the diffusion and surface reaction, and the physical properties and surface kinetic characteristics of major intermediate species (e.g., BHCl, AlCl, etc., as determined from the thermodynamic calculations) are similar to those of BCl_3 and $AlCl_3$.

(5) The Stefan-Maxwell equations required for a multi-component diffusion process are not needed here since the reactant mixture typically contains more than 90% Ar (i.e., pseudo-binary mixture). Then Fick's second law along with the pseudo binary diffusion coefficients (e.g., D_{i-Ar}) can be used to describe the molecular diffusion of BCl_3 and $AlCl_3$.

With the above assumptions, the diffusion equations for the molecular flux of species i, J_i, become:

$$J_{BCl_3} = \frac{D_{BCl_3-Ar}}{RT} \left(\frac{dP_{BCl_3}}{dz} \right) \tag{2}$$

$$J_{AlCl_3} = \frac{D_{AlCl_3-Ar}}{RT} \left(\frac{dP_{AlCl_3}}{dz} \right) \tag{3}$$

The first order approximation of the above equations gives:

$$J_{BCl_3} = \frac{D_{BCl_3-Ar}}{RT\ \delta_{BCl_3}} (P_{BCl_3} - P_{BCl_3}^{*}) \tag{4}$$

$$J_{AlCl_3} = \frac{D_{AlCl_3-Ar}}{RT\ \delta_{AlCl_3}} (P_{AlCl_3} - P_{AlCl_3}^{*}) \tag{5}$$

where P_i and P_i^* are the partial pressures of species i in the bulk gas phase and at the deposition surface, respectively, and δ_i is the concentration boundary layer thickness for species i. However,

based on assumptions (3) and (4), P_i can be substituted with the inlet partial pressure, $P_i°$, therefore

$$J_{BCl_3} = \frac{D_{BCl_3\text{-}Ar}}{RT\ \delta_{BCl_3}} (P_{BCl_3}° - P_{BCl_3}^*) \quad (6)$$

$$J_{AlCl_3} = \frac{D_{AlCl_3\text{-}Ar}}{RT\ \delta_{AlCl_3}} (P_{AlCl_3}° - P_{AlCl_3}^*) \quad (7)$$

Now the assumption of pseudo first order surface decomposition of BCl_3 and $AlCl_3$ gives:

$$J_{k,BN} = \frac{k_{BN}}{RT} P_{BCl_3}^* \quad (8)$$

$$J_{k,AlN} = \frac{k_{AlN}}{RT} P_{AlCl_3}^* \quad (9)$$

At steady state, the overall BN and AlN growth rates are:

$$J_{BN} = J_{BCl_3} = J_{k,BN} \quad (10)$$

$$J_{AlN} = J_{AlCl_3} = J_{k,AlN} \quad (11)$$

Combining Eqs. (6) through (11) gives:

$$J_{BN} = \frac{P_{BCl_3}°/RT}{\delta_{BCl_3}/D_{BCl_3\text{-}Ar} + 1/k_{BN}} \quad (12)$$

$$J_{AlN} = \frac{P_{AlCl_3}°/RT}{\delta_{AlCl_3}/D_{AlCl_3\text{-}Ar} + 1/k_{AlN}} \quad (13)$$

Although the above derivation is based on a simplified process description, it provides a fundamental basis for understanding the codeposition process. The phase composition of the BN+AlN composites is determined by the ratio of J_{BN} and J_{AlN}. The terms δ_i/D_{i-Ar} and $1/k_i$ can be thought of as "diffusion resistance" and "kinetic resistance" to the process, respectively. In other words, the process is limited by diffusion if δ_i/D_{i-Ar} is much larger than $1/k_i$ and is kinetically controlled if the opposite is true. The magnitude of δ_i/D_{i-Ar} can be easily estimated for the impinging jet geometry. The momentum boundary layer thickness is

$$\delta_m = 2.1\ (2\ \nu/a)^{1/2} \tag{14}$$

where a is a hydrodynamic constant which can be determined from correlations given in Chin and Tsang [38] and ν is the kinematic viscosity. The concentration boundary layer thickness, δ_i, can be approximated by [45]:

$$\delta_i = \delta_m/(Sc_i)^{1/3} \tag{15}$$

where $Sc_i = \nu/D_{i-Ar}$.

The effect of temperature on the overall growth rate can also be understood from the above model. The diffusional flux is a weak function of temperature because:

$$D_{i-Ar} \propto T^{5/3} \tag{16}$$

and

$$\delta_i \propto 1/Sc^{1/3} \propto D_{i-Ar}{}^{1/3} \propto T^{5/9} \tag{17}$$

so

$$J_i \propto D_{i-Ar}/(T\delta_i) \propto T^{1/9} \tag{18}$$

However, the kinetic flux is exponentially dependent on temperature. The combination of the two fluxes is responsible for the

typical deposition rate versus temperature relationship observed in many CVD systems. The deposition rate increases exponentially with temperature within a low temperature region (i.e., kinetically controlled). At higher temperatures the process becomes limited by a slow increase in the diffusional flux resulting in the saturation of the deposition rate.

Crystal Nucleation and Growth

The previous section was concerned with the rate of deposition. To a large extent, the same factors (e.g., temperature, pressure, reactant concentrations) which control the deposition rate also influence nucleation and growth of the deposit and, therefore, its microstructure. During the CVD process, molecules arrive at the deposition surface from the gas phase by molecular diffusion and undergo chemical decompositions and reactions at the surface. Subsequently, as newly formed adatoms (i.e., products) diffuse over the deposition surface, small stable clusters of the adatoms nucleate, grow, and coalesce. In order for the growth to occur, condensation of the adatoms should be favored over evaporation. This means that the small clusters must be larger than a critical size according to the classical nucleation theory [46,47]:

$$r^* = \frac{2\gamma V}{kT \ln(P/P_{eq})} \qquad (19)$$

where γ is the specific surface energy and V is the atomic volume. However, in most CVD processes, the supersaturation term, $T \ln(P/P_{eq})$, is so high that the critical cluster size approaches molecular dimensions (i.e., 1 to 8 atoms) [48-51]. It is defined here that P is the partial pressure of the adatoms at the deposition surface and P_{eq} is the equilibrium vapor pressure of the atoms in the gas phase. In the case of such small critical clusters, a statistical-mechanical treatment is required to describe the

nucleation process [48]. The density of the critical clusters, N_n^*, is given by:

$$N_n^*/N_o = (N_1/N_o)^n \exp(E_n/kT) \quad (20)$$

where N_o is the number of the adsorption sites, N_1 is the number of the surface adatoms, and E_n is the net energy gain on forming the cluster containing n adatoms. Furthermore, the nucleation rate, I, is [48,52]:

$$I = N_n^* r_n^* N_1 u \quad (21)$$

and

$$u = zf \exp(-E_d/kT) \quad (22)$$

where σ_n^* is the capture width of the critical nucleus, u is the surface mobility of the adatoms, z is the number of adjacent sites, f is the total jump frequency, and E_d is the activation energy for surface diffusion. The nucleation behavior of simple deposition systems such as sputter deposition of Au and CVD of Si has been examined using this statistical-mechanical approach in a somewhat quantitative manner. In general, however, such quantitative treatment is a formidable task for most CVD systems due to their complexity and the experimental difficulties in verifying proposed nucleation mechanisms.

In practice, three major types of heterogeneous nucleation can be qualitatively described using this statistical-mechanical approach. First, amorphous growth is usually obtained when non-volatile adatoms are formed at a relatively high rate (i.e., high deposition rate) and the surface diffusion of these adatoms is slow (i.e., low deposition temperature). This is because: "a newly created adatom impinges on a specific site before the previously formed adatoms have made a sufficient number of diffusional jumps to reach energetically more favorable crystallographical sites" [51]. When the mobility of the adatoms becomes sufficiently high

as temperature increases, formation of a polycrystalline structure results. Furthermore, when temperature is increased to a point where the process becomes diffusion-limited, epitaxial or/and single crystal growth takes place. This occurs because the mobility of the adatoms increases exponentially with temperature according to Eq. (22) whereas the increase in the deposition rate becomes a weak function of temperature in the diffusion-limited region according to Eq. (18). In addition to these major types, a layered crystalline structure is often deposited when adhesive forces between the adatoms and the deposition surface are stronger than cohesive forces among the adatoms [50,51].

Therefore, nucleation behavior is primarily influenced by temperature which affects the mobility of the adatoms as well as the deposition rate. However, other operating conditions such as pressure and reactant concentrations can also influence the final crystal structure by altering the deposition rate. For example, when pressure and reactant concentrations are changed to increase the deposition rate of silicon, the crystallinity of silicon is found to decrease [50]. The following equation shows the general relationship between the final crystal structure, C, of CVD coatings and the operating conditions:

$$C = f \{ J_G(T,P,P_i), \quad u(T) \} \tag{23}$$

The above correlation is based on experimental observations from the CVD of single phase systems. To date, CVD of dispersed phase composites has not been studied enough to answer a basic, but important question: how should the simultaneous nucleation and growth of two chemically different and/or competing phases (i.e., BN and AlN) be treated? Nevertheless, it is expected that the qualitative nature of the aforementioned nucleation and growth theory is still applicable to the proposed BN+AlN composite system and, therefore, will be used in interpreting the microstructure of the composites in terms of operating conditions.

Future Modeling

As stated earlier, the purpose of this study is to enhance the basic understanding of the codeposition of dispersed phase ceramic composites, specifically that of BN and AlN, by developing a qualitative model which relates the operating conditions such as temperature and reactant concentrations to the microstructure of the deposit. This requires a detailed understanding of the kinetics of the BN+AlN system, which is complicated by the mass transfer limitation frequently encountered in the high temperature CVD environment. After the kinetic/mass transfer behavior is understood, the statistical-mechanical crystal nucleation and growth theory can be applied to establish the relationship between the kinetics of the system and the microstructure.

In general these two are related as follows. In an impinging jet geometry the deposition rate of BN or AlN is determined by the kinetics of the BN+AlN as previously discussed:

$$J_{BN} = f(T, P, P_i, v) \tag{24}$$

$$J_{AlN} = g(T, P, P_i, v) \tag{25}$$

where f and g are the rate equations such as the Langmuir-Hinshelwood type coupled with the mass transfer terms, or simply an empirical power expression. P_i and v are the inlet partial pressure of reactant i and the linear fluid velocity, respectively. The crystal structure, C , (i.e., crystallinity and crystallite size) of BN or AlN in the case of single phase deposition (i.e., BN-CVD or AlN-CVD) is governed by the following parameters.

$$C_{BN} = p(u_i, J_{BN}) \tag{26}$$

$$C_{AlN} = q(u_i, J_{AlN}) \tag{27}$$

where u_i is the surface mobility of adatoms i and is exponentially dependent on temperature (see Eq. 22). However, Eqs. (26) and (27) are derived for single phase deposition systems. The solution to this problem is the hypothesized growth mechanism for two competing phases which was originated during the course of research. The main idea behind this hypothesis is that the codeposition of two chemically different phases is a competitive process in which the growth of one phase interferes with and limits the growth of the other. Then Eqs. (26) and (27) become in the case of the codeposition process:

$$C_{BN} = v\,(u_i,\ J_{BN},\ J_{AlN}) \tag{28}$$

$$C_{AlN} = w\,(u_i,\ J_{AlN},\ J_{BN}) \tag{29}$$

This modeling approach, which links the kinetics to the crystal nucleation and growth behavior in the codeposition of dispersed phase ceramics, has been successful in interpreting the experimental results already discussed.

There are two major areas to be emphasized for the successful completion of this research: (1) understanding of the kinetic behavior of BN-CVD, AlN-CVD, and most importantly BN+AlN-CVD by preparing these materials over a wide range of operation conditions in the impinging jet geometry and (2) extensive characterization of the coatings using electron microprobe, ESCA, SEM, TEM/STEM and XRD. The BN-CVD and AlN-CVD systems will be separately investigated using the same modeling concept, but in a somewhat less rigorous fashion, in order to compare the deposition behavior of these systems with that of the BN+AlN-CVD. It is recognized that the complexity of the BN+AlN-CVD is too great to permit understanding of its deposition behavior without first realizing the kinetic and growth mechanisms of the BN-CVD and AlN-CVD.

VI. CONCLUSIONS

Dispersed phase composites containing BN+AlN were deposited by CVD. The phases were either amorphous or crystalline depending on the deposition temperature and reagent concentration. One type of deposit which consisted of a turbostratic BN matrix containing oriented single crystal whiskers of AlN was very hard.

A qualitative model based on statistical-mechanical nucleation theory and a hypothesized competition between growth of BN and AlN phases was successful in describing the relationship between operating conditions and the resulting microstructure of dispersed phase ceramic (BN+AlN) composites prepared by CVD. This ability to control the microstructure offers a promising future for this CVD composite system. The present study has provided a fundamental basis for developing more quantitative models, which will integrate the underlying principles of thermodynamics, kinetics, transport phenomena, nucleation and crystal growth theory.

REFERENCES

1. W.J. Lackey, A.W. Smith, D.M. Dillard, and D.J. Twait, "Codeposition of Dispersed Phase Ceramic Composites," pp. 1008-1027 in Proceedings of the 10th International Conference on Chemical Vapor Deposition, ed. G.W. Cullen, The Electrochemical Society, Inc., Pennington, NJ, 1987.

2. N.J. Archer, "The Preparation and Properties of Pyrolytic Boron Nitride," pp. 167-180 in High Temperature Chemistry of Inorganic and Ceramic Materials, ed. F.P. Glassen and P.E. Potter, The Chemical Society, Burlington House, London, 1976.

3. G. Clerc and P. Gerlach, "Pyrolytic Boron Nitride," pp. 777-785 in Proceedings of the 5th International Conference on Chemical Vapor Deposition, ed. J.M. Blocher et al., The Electrochemical Society, Princeton, NJ, 1975.

4. C.E. Frahme, "The Chemical Vapor Deposition of Pyrolytic Boron Nitride," Ph.D. Dissertation, Rutgers University, 1966.

5. H. Tanji, K. Monden, and M. Ide, "CVD Mechanism of Pyrolytic Boron Nitride," pp. 562-569 in Proceedings of the 10th International Conference on Chemical Vapor Deposition," ed. G.W. Cullen, The Electrochemical Society, Pennington, NJ, 1987.

6. G. Malé and D. Salanoubat, "Preparation of Pyrolytic Boron Nitride (PBN) by CVD at Reduced Pressure," pp. 391-397 in Proceedings of the 7th International Conference on Chemical Vapor Deposition, ed. T.O. Sedgwick and H. Lydtin, The Electrochemical Society, Princeton, NJ, 1979.

7. S. Motojima, Y. Tamura, and K. Sugiyama, "Low Temperature Deposition of Hexagonal BN Films by Chemical Vapor Deposition," Thin Solid Films, 88, 269 (1982).

8. T. Takahashi, H. Itoh, and A. Takeuchi, "Chemical Vapor Deposition of Hexagonal Boron Nitride Thick Film on Iron," J. Crystal Growth, 47, 245 (1979).

9. T. Takahashi, H. Itoh, and M. Kuroda, "Structure and Properties of CVD-BN Thick Film Prepared on Carbon Steel Substrate," J. Crystal Growth, 53, 418 (1981).

10. M. Sano and M. Aoki, "Chemical Vapor Deposition of Thin Films of BN onto Fused Silica and Sapphire," Thin Solid Films, 83, 247 (1981).

11. T. Matsuda, N. Uno, H. Nakae, and T. Hirai, "Synthesis and Structure of Chemically Vapour Deposited Boron Nitride," J. Mater. Sci., 21, 649 (1986).

12. T. Matsuda, H. Nakae, and T. Hirai, "Density and Deposition Rate of Chemical Vapour Deposited Boron Nitride," J. Mater. Sci., 23, 509 (1988).

13. M. Morita, N. Uesugi, S. Isogai, K. Tsubouchi, and N. Mikoshiba, "Epitaxial Growth of Aluminum Nitride on Sapphire Using Metalorganic Chemical Vapor Deposition," Japanese J. Appl. Phys., 20, 17 (1981).

14. W.M. Yim, E.J. Stofko, P.J. Zanzucchi, J.I. Pankove, M. Ettenberg, and S.C. Gilbert, "Epitaxially Grown AlN and Its Optical Band Gap," J. Appl. Phys., 44, 292 (1973).

15. J. Bauer, L. Biste, and D. Bolze, "Optical Properties of Aluminum Nitride Prepared by Chemical and Plasmachemical Vapour Deposition," Phys. Stat. Sol., a39, 173 (1977).

16. M. Suzuki and H. Tanji, "CVD of Polycrystalline Aluminum Nitride," pp. 1089-1097, in Proceedings of the 10th International Conference on Chemical Vapor Deposition, ed. G.W. Cullen, The Electrochemical Society, Inc., Pennington, NJ, 1984.

17. Y. Pauleau, A. Bouteville, J.J. Hantzpergue, J.C. Remy, and A. Cachard, "Thermodynamics and Kinetics of Chemical Vapor Deposition of Aluminum Nitride Films," J. Electrochem. Soc., 127, 1532 (1980).

18. Y. Chubachi, K. Sato, and K. Kojima, "Reflection High Energy Electron Diffraction and X-ray Studies of AlN Films Grown on Si(111) and Si(001) by Organometallic Chemical Vapour Deposition," Thin Solid Films, 122, 259 (1984).

19. H. Arnold, L. Biste, D. Bolze, and G. Eichhorn, "Chemical and Plasmachemical Vapour Deposition of Aluminum Nitride Layers," Kristall and Technik, 11, 17 (1976).

20. K.S. Mazdiyasni, R. Ruh, and E.E. Hermes, "Phase Characterization and Properties of AlN-BN Composites," Am. Ceram. Soc. Bull., 64, 1149 (1985).

21. T.M. Besmann, "SOLGASMIX-PV, A Computer Program to Calculate Equilibrium Relationships in Complex Chemical Systems," ORNL/TM-5775, Oak Ridge National Laboratory, Oak Ridge, TN, April 1977.

22. D.J. Twait, W.J. Lackey, A.W. Smith, and W.Y. Lee, "Thermodynamic Analysis of the Chemical Vapor Deposition of BN+AlN Composite Coatings," to be submitted to J. Am. Cer. Soc. (1989).

23. J.W. Daily and D.R.F. Harleman, "Fluid Dynamics," Addison-Wesley Co., Massachusetts, 1966.

24. J. Thomas, N.E. Weston, and T.E. O'Conner, "Turbostratic Boron Nitride, Thermal Transformation to Ordered-Layer-Lattice Boron Nitride," J. Am. Chem. Soc., 84, 4619 (1963).

25. D. Walton, "Nucleation of Vapor Deposits," J. Chem. Phys., 37, 2182 (1962).

26. B. Lewis and D.S. Campbell, "Nucleation and Initial Growth Behavior of Thin-Film Deposits," J. Vac. Sci. Tech., 4, 209 (1967).

27. J. Bloem, "Nucleation of Silicon on Amorphous and Crystalline Substrates," pp. 41-58 in Proceedings of the 7th International Conference on Chemical Vapor Deposition, ed. T.O. Sedgwick and H. Lydtin, The Electrochemical Society, Princeton, NJ, 1979.

28. R.F. Davis, "Interfacial Phenomena during Chemical Vapor Deposition," pp. 379-390 in Materials Science Research Vol. 14, ed. J. Pask and A. Evans, Prenium Press, New York, 1981.

29. W.J. Lackey, G.B. Freeman, A.W. Smith, J.R. Thompson, G.J. Gérard, P.K. Agrawal, W.Y. Lee, and D.J. Twait, "Ultrafine Microstructure Composites Prepared by Chemical Vapor Deposition," Annual Report, A-4699-1, Georgia Tech Research Institute, January 1988.

30. D.W. Hess, K.F. Jensen, and T.J. Anderson, "Chemical Vapor Deposition: A Chemical Engineering Perspective," Rev. Chem. Eng., 3, 97 (1985).

31. K.F. Jensen, "Modeling of Chemical Vapor Deposition Reactors", pp. 3-20 in Proceedings of the 9th International Conference on Chemical Vapor Deposition, ed. McD Robinson et al., The Electrochemical Society, Pennington, NJ, 1984.

32. H. Rebenne and R. Pollard, "Theoretical Analysis of Chemical Vapor Deposition of Ceramics in an Impinging Reactor," J. Am. Ceram. Soc., 70, 907 (1987).

33. L. Vandenbulcke, "Mass Transfer, Equilibrium, and Kinetics in the CVD of a Polycomponent System: Application to Boron-Carbon," pp. 315-331 in Proceedings of the 7th International Conference on Chemical Vapor Deposition, ed., T.O. Sedwick and H. Lydtin, The Electrochemical Society, Princeton, NJ, 1979.

34. L. Vandenbulcke and G. Vuillard, "Kinetics in Chemical Vapor Deposition of Boron Carbide," pp. 95-103 in Proceedings of the 8th International Conference on Chemical Vapor Deposition, ed. J.M. Blocher et al., The Electrochemical Society, Pennington, NJ, 1981.

35. K.F. Roenigk and K.F. Jensen, "Analysis of Multicomponent LPCVD Processes: Deposition of Pure and In-Situ Doped Poly-Si," J. Electrochem. Soc., 132, 448 (1985).

36. K.F. Roenigk and K.F. Jensen, "Low Pressure CVD of Silicon Nitride," J. Electrochem. Soc., 125, 1461 (1987).

37. G.F. Froment, "Model Discrimination and Parameter Estimation in Heterogeneous Catalysis", AIChE J., 21, 1041 (1975).

38. D-T. Chin and C-H. Tsang, "Mass Transfer to an Impinging Jet Electrode," J. Electrochem. Soc., 125, 1461 (1978).

39. H. Schlichting, "Boundary Layer Theory," pp. 70-73, McGraw-Hill Book Co., New York, 1955.

40. J.W. Daily and D.R.F. Harleman, "Fluid Dynamics," Addison-Wesley Co., Massachussettts, 1966.

41. C. Houtman, D.B. Graves, and K.F. Jensen, "CVD in Stagnation Point Flow," J. Electrochem. Soc., 133, 961 (1986).

42. L. Vandenbulcke and G. Vuillard, "Chemical Vapor Deposition of Boron on Massive Substrates," J. Electrochem. Soc., 123, 278 (1976).

43. M. Michaelidis and R. Pollard, "Analysis of Chemical Vapor Deposition of Boron," J. Electrochem. Soc., 131, 860 (1984).

44. G. Wahl, "Hydrodynamic Description of CVD Processes," Thin Solid Films, 40, 13 (1977).

45. R.B. Bird, W.E. Stewart, E.M. Lightfoot, "Transport Phenomena," pp. 606-608, Wiley and Sons, New York, 1960.

46. J.P. Hirth and G.M. Pound, "Condensation and Evaporation-Nucleation and Growth Processes," Pergamon Press, NY, 1966.

47. W.D. Kingery, H.K. Bowen, and D.R. Uhlman, "Introduction to Ceramics," 2nd ed., John Wiley & Sons, New York, 1976.

48. D. Walton, "Nucleation of Vapor Deposits," J. Chem. Phys., 37, 2182 (1962).

49. B. Lewis and D.S. Campbell, "Nucleation and Initial Growth Behavior of Thin-Film Deposits," J. Vac. Sci. Tech., 4, 209 (1967).

50. J. Bloem, "Nucleation of Silicon on Amorphous and Crystalline Substrates," pp. 41-58 in Proceedings of the 7th International Conference on Chemical Vapor Deposition, ed. T.O. Sedgwick and H. Lydtin, The Electroechemical Society, Princeton, NJ, 1979.

51. R.F. Davis, "Interfacial Phenomena during Chemical Vapor Deposition," pp. 379-390 in Materials Science Research Vol. 14, ed. J. Pask and A. Evans, Prenium Press, New York, 1981.

52. G.A. Somorjai, "Principles of Surface Chemistry," pp. 101-105, Prentice-Hall, Englewood Cliffs, NJ, 1972.